

THE PENNSYLVANIA STATE UNIVERSITY  
MILLENNIUM SCHOLARS PROGRAM

DEPARTMENT OF SCIENCE

A COMPUTATIONAL MODEL OF STRAIN AND RATE-DEPENDENT NEURONAL  
INJURY

PATRICIA YVETTE DE TOMAS-MEDINA  
SPRING 2018

A thesis  
submitted in partial fulfillment  
of the requirements  
for a baccalaureate degree  
in Science  
with honors in Science

Reviewed and approved\* by the following:

Reuben H. Kraft  
Shuman Assistant Professor of Mechanical Engineering  
Thesis Supervisor

Ronald A. Markle  
Professor of Biology  
Honors Adviser

\* Signatures are on file in the Millennium Scholars Program Office.

## ABSTRACT

In the United States alone, over 1.7 million cases of traumatic brain injury are reported annually. The prevalence of these injuries and their effects have greatly increased the need for understanding the mechanisms of neuronal deformation during injurious loading.

Previously, specially designed in vitro experiments of compressive neuronal deformation demonstrated that at different strain loading magnitudes and rates influence injury pathology differently. For example, magnitude affects the time of neuronal death, while strain rate influences the pathomorphology and extent of injury. While these experimental findings are valuable, there are still challenges in resolving fine details of the strain distribution in the cell during loading due to geometry-based stress concentrations. Therefore, the objective of this effort is to develop a high-resolution computational model of neuronal deformation that will enable us to compute strains throughout the cell.

Using high resolution images of a single neuron enables the inclusion of all major components of the neuronal cell, including the tortuous axons and dendrites. In the experimental settings, the cell is immersed in a collagen gel which play a role in the mechanical response. In our computational model, both the gel and the neuron are included using an embedded constraint. The process of cellular segmentation, surface improvement and final finite element meshing took extensive work, and the process from experimental results to dynamic model will be discussed. The time-dependent simulation and the experimental results will be compared and we will highlight areas where the computational simulation help elucidate fine details of the strain and injury correlations.

## TABLE OF CONTENTS

<u>LIST OF FIGURES .....</u>	<u>iii</u>
<u>LIST OF TABLES .....</u>	<u>iv</u>
<u>ACKNOWLEDGEMENTS .....</u>	<u>v</u>
Chapter 1 Introduction .....	1
Background .....	1
Motivation .....	7
Chapter 2 Dynamic Finite Element Analysis Process .....	10
The Computational Modeling Process .....	10
Creating a Segmented Surface: Avizo .....	12
Computer Aided Design: Blender .....	15
Finite Element Meshing: ANSYS ICEM-CFD .....	16
Chapter 3 Numerical Computational Simulation: LS-DYNA .....	18
Keyword Modification .....	19
Simulation Times and Completion Percentage .....	21
Chapter 4 Computational Modeling Results .....	22
Chapter 5 Conclusion .....	25
Discussion .....	25
Application .....	26
GitHub .....	27
Appendix A Finite Element Analysis .....	28
LS-DYNA 10 s <sup>-1</sup> Simulation Keyword File .....	28
LS-DYNA 75 s <sup>-1</sup> Simulation Keyword File .....	31
BIBLIOGRAPHY .....	36

## LIST OF FIGURES

Figure 1 Experimental device setup <sup>3</sup> .....	2
Figure 2 Morphological injury after compressive loading <sup>3</sup> .....	4
Figure 3 Cells exhibiting blebbing <sup>3</sup> .....	5
Figure 4 Relationship between time of cell death and local axial strain <sup>3</sup> .....	5
Figure 5 Aaron Hernandez CTE affected brain in comparison to normal tissue <sup>10</sup> .....	7
Figure 6 Computational Modeling Phases.....	9
Figure 7 Neuronal network stained with Calcein AM <sup>3</sup> .....	11
Figure 8 Single neuron highlighted using COL-I <sup>3</sup> .....	11
Figure 9 Flow diagram of modeling process .....	12
Figure 10 Slices from the stack of images acquired from the Franck Lab .....	13
Figure 11 Segmentation surface created using Avizo .....	13
Figure 12 Surface from Avizo imported into ANSYS ICEM-CFD meshing software.....	14
Figure 13 Gaps in imported surface.....	14
Figure 14 Fixing holes in Blender .....	15
Figure 15 Final Blender edited neuron .....	16
Figure 16 Full volume rendition of mesh created in ANSYS ICEM-CFD .....	17
Figure 17 Neuronal mesh embedded in a created gel.....	18
Figure 18 Dimensions of simulation.....	19
Figure 19 High strain rate model .....	22
Figure 20 Low strain rate model.....	22
Figure 21 Pressure of high strain rate model .....	23
Figure 22 Pressure of low strain rate model .....	23
Figure 23 Pressure graph corresponding to elements in low strain rate model .....	24
Figure 24 Comparison of high and low strain rate model principal strains.....	24

Figure 25 Visual flow diagram of modeling process.....	25
--	----

## LIST OF TABLES

Table 1 Computational Modeling Process Overview .....	11
---	----

## **ACKNOWLEDGEMENTS**

This publication and research would not have been possible without the help and support of several people. I would first like to thank all of the members and faculty involved with the Penn State Computational Biomechanics Group. A special thank you goes to Dr. Reuben Kraft, the head of the group, and all of his graduate students who I have worked with over the past years and welcomed me into such an enriching environment. This research also benefited from the support from Christian Franck and his research group at Brown University. I would also like to thank Dr. Ronald Markle for his role as my honors advisor. In addition, I would like to thank Vikram Subramani for guiding me through troubleshooting my simulations. Lastly, I would like to thank my family for their understanding and support while I worked on this project at the Pennsylvania State University in University Park, PA.

## **Chapter 1**

### **Introduction**

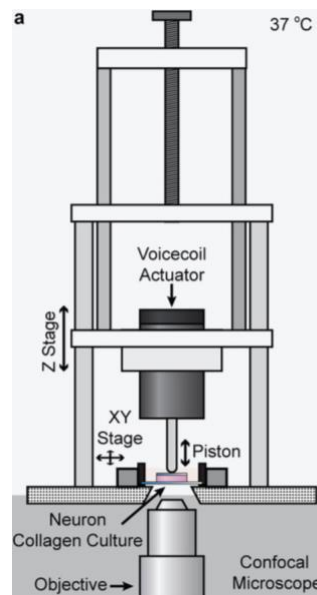
The traumatic brain injury crisis in the United States has created a great demand for understanding the mechanics of injury. In the United States alone, 1.7 million cases of traumatic brain injury are reported yearly<sup>1</sup>. Evidence shows that the prevalence and magnitude of these injuries can lead to many behavior changes in addition to life altering diseases including Alzheimer's, Parkinson's, and Chronic Traumatic Encephalopathy as well as motor neuron disease<sup>2</sup>. Understanding the mechanisms of traumatic brain injury at the neuronal level is crucial for enhancing treatment and diagnosis of injury. In addition, information is lacking regarding predictive correlation of injury and strain. In this chapter, evidence found at the experimental level that served as the basis for this research will be explained. This chapter will also include more information regarding the importance and motivation for partaking in this research.

### **Background**

Traumatic brain injury often results in the death of many neurons. Most of these result from compressive deformation as a result of blunt head traumas. These neuronal deaths can have immense impact on the behavior and well-being of a patient in both the long and short term. Understanding these injuries and creating computational models can help personalize care, diagnosis, and determine prognosis for patients.



The Franck Lab at Brown University has developed an *in vitro* model of neuronal injury in order to investigate the role of mechanoporation, shear, and axial deformations in neurons subjected to compressive loading. Many models dealing with traumatic brain injury and spinal cord injuries have been developed through the Penn State Computational Biomechanics group. Though models exist for low strain rate injury at the cellular level, computational models replicating this high strain rate compression are still lacking. Given that trauma blunts occur at high strain rates, it is important to develop a computational model that is able to analyze neuron injury from a mechanical perspective. Strain and rate have been found to have significant impact on neuronal death. Strain magnitude affects timing of neuronal death, while strain rate influences the pathomorphology as well as how much the injury propagates to the surrounding population of cells<sup>3</sup>. A 3D cellular *in vitro* model of neuron injury looked at the deformations of a neuron subjected single compressive impacts. When subjected to different strain rates, morphology of injury varied drastically.



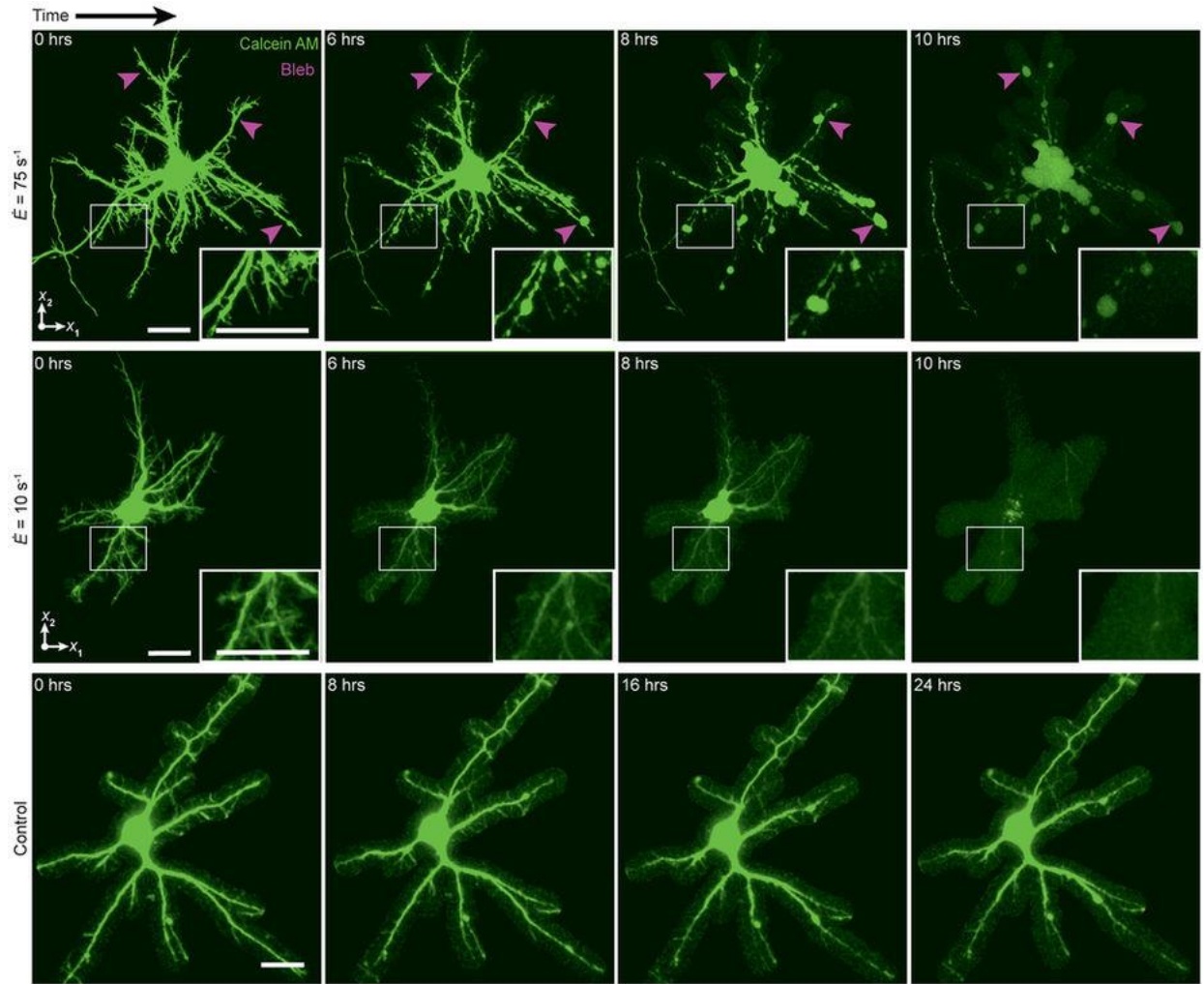
**Figure 1** Experimental device setup<sup>3</sup>

The Franck Lab was able to develop a high-resolution, *in-situ* 3D neuronal compression device. This device allowed for administering controlled and repeated uniaxial deformations to neurons embedded in a 3D collagen gel<sup>3</sup>. In order to create a continuous timeline of the experiment, the device was placed directly above a laser scanning confocal microscope. Figure 1. shows an animated representation of the experiment. Using a previously developed algorithm it was experimentally verified that all of the applied strain fields were the same throughout the imaging body.

This newly developed *in vitro* model of neuronal injury was developed and used in order to investigate the role of mechanoporation, shear, and axial deformations in neurons when subjected to single compressive impacts<sup>3</sup>. Models can be helpful in many ways and computational models can enhance this even more. In the experiments, neurons embedded in collagen gels were subjected to three different loading regimes. These were  $10^{-4} \text{ s}^{-1}$ , representing quasi-static movement,  $10 \text{ s}^{-1}$  and  $75 \text{ s}^{-1}$ . Previous traumatic brain injury investigations had found that the dynamically applied strain magnitude was 0.30 while the peak strain rates were  $10 \text{ s}^{-1}$  and  $75 \text{ s}^{-1}$ , which were used in the computational models created<sup>3</sup>.

When the experiment was conducted, it was found that many common morphological traumatic brain injury indicators including blebbing, retraction, and thinning of the neurites occurred<sup>3</sup>. Two unique neuropathomorphologies were found. The first was structural damage. This included changes within the cytoskeleton of the neurons. Once structural damage was visible, deterioration of the cytoskeleton came soon after very quickly. This often ended in cell death. Cell death was marked with the lysing of the cell or complete cellular fragmentation<sup>3</sup>. Lysing involves the failure of cellular structural components leading to the destruction of cellular processes keeping the cell alive through necrosis, or ultimate cell death<sup>4</sup>. The two different

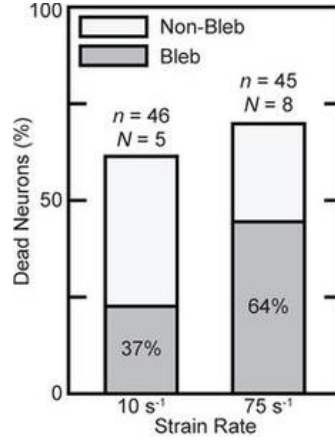
loading regimes exhibited different injury patterns. When exposed to  $\dot{\epsilon} = 10 \text{ s}^{-1}$ , the neurons showed gradual retraction and thinning of the axon and dendrites attached to the soma, which then ultimately lead to the lysing of the cell. On the other hand, when exposed to  $\dot{\epsilon} = 75 \text{ s}^{-1}$ , in addition the thinning and retracting morphology, the extensions also exhibited visible blebbing along neurites<sup>3</sup>. These differences can be seen in Figure 2.



**Figure 2 Morphological injury after compressive loading<sup>3</sup>**

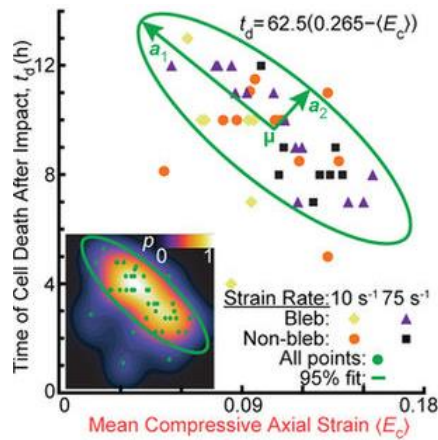
It was found that when increasing the strain from  $10 \text{ s}^{-1}$  to  $75 \text{ s}^{-1}$ , there was a 170% increase in the occurrence of blebbing. This difference can be seen in Figure 3 where  $N$  = the number of experiments and  $n$  = number of cells. When exposed to the  $10 \text{ s}^{-1}$ , only 37% of the

dead neurons experienced blebbing while when exposed to  $75 \text{ s}^{-1}$ , 64% of the dead neurons formed blebs<sup>3</sup>. As seen in Figure 2, the neurons compressed at a slow, quasi-static rate, resembled a control where no injury or morphological changes were observed.



**Figure 3 Cells exhibiting blebbing<sup>3</sup>**

This still did not give an answer to direct correlation between blebbing and cell death, since only 32% of all dead cells exhibited blebbing<sup>3</sup>. It was found that neither the shear nor axial strain correlated with the presence of morphological features. The relationship found was of that between time of death ( $t_d$ ) and local axial strain. The relationship can be described by the equation  $t_d = 62.5(0.265 - \langle E_c \rangle)^3$ . These relationships can be seen in the ellipse distribution in Figure 4.



**Figure 4 Relationship between time of cell death and local axial strain<sup>3</sup>**

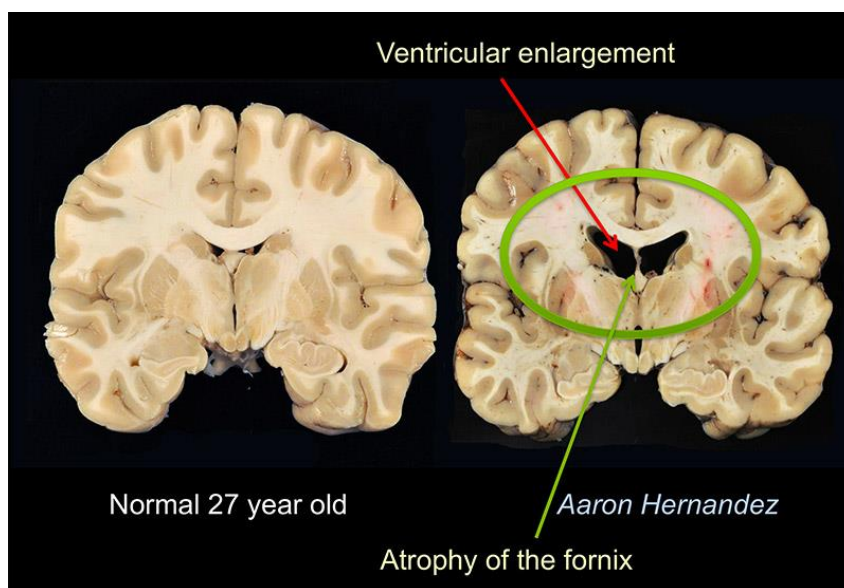
Using cell permeable fluorescent dye (Alexa Fluor 568 hydrazide), mechanoporation was detected. The intensity of the dye was compared amongst the impact strain rates of  $10 \text{ s}^{-1}$  and  $75 \text{ s}^{-1}$  and a control. The time of peak intensity was compared in each situation. Lysis of the cell was characterized by both leaking of live cell dye Calcein AM and extreme morphological deformities<sup>3</sup>. Contrary to many experiments before, it was found that Alexa Fluor 568 Hydrazide inflow actually only occurred at the time of cell death<sup>3</sup>. Other experiments had previously found that shear-and stretch- injury models that permeability of membranes steadily increased after impact loading<sup>5,6,7,8</sup>.

The two observed loading rates exhibited very different pathomorphologies. This is important because it indicates different forms of injury with increasing impact rate<sup>3</sup>. Though not used in this research, but will be a factor for future modeling, there is a disruption in neurite transport involving the accumulation of vesicles and organelles within the cell, which leads to the formation of blebbing<sup>9</sup>.

This research served to become the first step in replicating this experiment with a computational finite element model. It sought to replicate the compression model on a single neuron and then observe the local axial and shear strain rates. Using segmenting, meshing, and modeling techniques, as well as high resolution images provided by the Franck Lab, this research created a compression model with at the strain rates of  $10 \text{ s}^{-1}$  and  $75 \text{ s}^{-1}$  and local strains were analyzed and compared to the data presented by the Franck Lab.

## Motivation

Traumatic brain injury results in 1.7 million cases a year on average in the United States alone. These injuries often result from blunt head traumas and account for 52,000 deaths, 275,000 hospitalizations, and over one million emergency department visits<sup>1</sup>. Though commonly associated with sports injuries, these traumas include falling, motor vehicle accidents, and being struck by or against something (i.e. colliding in sports, assault, combat, etc.)<sup>1</sup>. Among these children have a high risk of injury and negative post-concussion due to their developing brains. Traumatic brain injury is a contributing factor to nearly of third of injury related deaths in the United States<sup>1</sup>.



**Figure 5 Aaron Hernandez CTE affected brain in comparison to normal tissue<sup>10</sup>**

One of the greatest concerns with repetitive brain injury is the occurrence of neurodegenerative diseases including chronic traumatic encephalopathy or CTE. These diseases are often found in athletes, military veterans, and many other people who experience repetitive head injuries throughout their lives<sup>10</sup>. It is characterized by clumping of Tau protein that slowly spreads and kills the surrounding cells in the brain<sup>10</sup>. Boston University's CTE Center analyzed

the brain tissue of former NFL player Aaron Hernandez after his death. It was found that Aaron Hernandez had the most severe CTE in a young person that researchers at Boston University had ever seen<sup>11</sup>. Figure 5 shows a comparison of Aaron Hernandez's brain to that of healthy brain tissue. CTE can have an effect on a person's mood or behavior including changes in aggression, depression, and paranoia<sup>10</sup>. CTE can only be diagnosed after death, when brain tissue can be sliced and visible clumps can be detected. Modeling can serve as the future of diagnosing and better understanding diseases including and similar to CTE.

Computational modeling can be seen as two phases. The first is understanding and the latter is predictive. This model serves as a starting point, having representative material properties of both a neuron and the collagen gel which they were embedded in during the *in vitro* experiment. Figure 6 shows the flow, division, and implementation of future phases.

The Penn State Computational Biomechanics lab is dedicated to creating several understanding and predictive models of both injury and disorders spread throughout the human body. Many of these models include brain and spinal injury models. Many models exist for full brain, but by examining this problem at the neuronal level, it will serve as a large stepping stone in understanding why the brain acts the way it does. By creating a model that focuses on neurons, it will be useful in creating more accurate predictive models of the entire brain being subjected to dynamic loading.


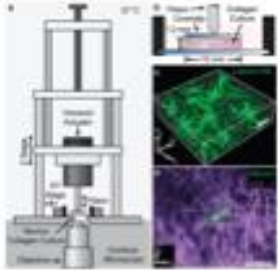
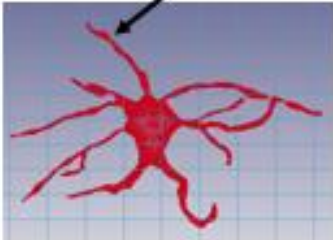
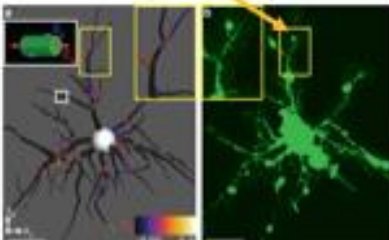
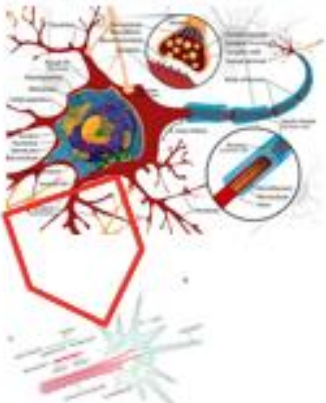
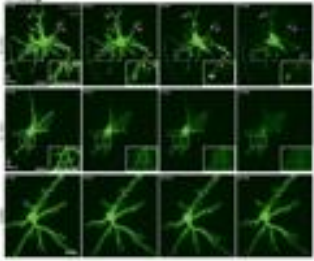
	Model	Experiment
<b>Phase I: Understanding</b>		
	<p>Local Injury and Strain Rate</p> 	<p>Local Injury and Strain Rate</p> 
<b>Phase II: Predicting</b>	<p>Implementing Organelles, Proteins, and Neuron Structures within the Model</p> 	

Figure 6 Computational Modeling Phases



## Chapter 2

### Dynamic Finite Element Analysis Process

After establishing the ground work involving the discoveries of the *in vitro* experiment conducted at Brown University, and its importance it is now important to discuss the software which was used to create this computational model. These next few sections will outline the critical steps and phases involved in transitioning from an *in vitro* model to a computational model.

### The Computational Modeling Process

In order to replicate the experiments conducted at Brown University in order to observe local axial and sheer strains amongst parts of a single neuron, several steps had to be taken in order to give us accurate numerical values. The model is an embedded model representing the setup seen in Figure 1. This was made possible through images sent from the Franck Lab of a single neuron in a larger cluster embedded in the gel. The cluster of neurons stained with Calcein AM embedded in the collagen gel can be seen in Figure 7. Figure 8 shows a single neuron highlighted with COL-I in the network of cells.

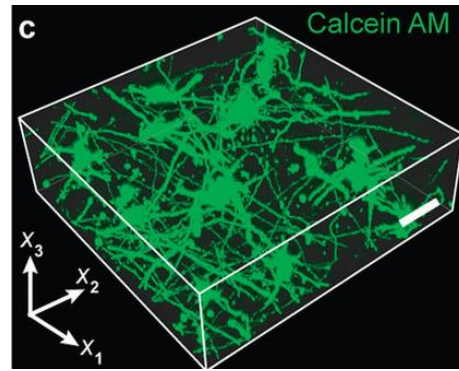


Figure 7 Neuronal network stained with Calcein AM<sup>3</sup>

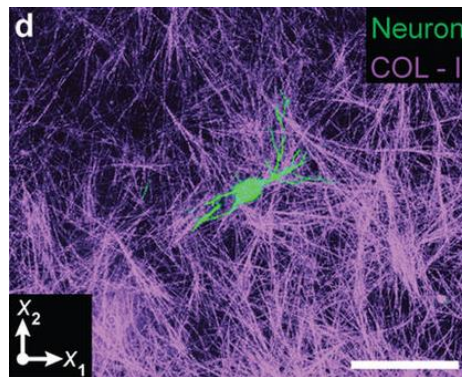
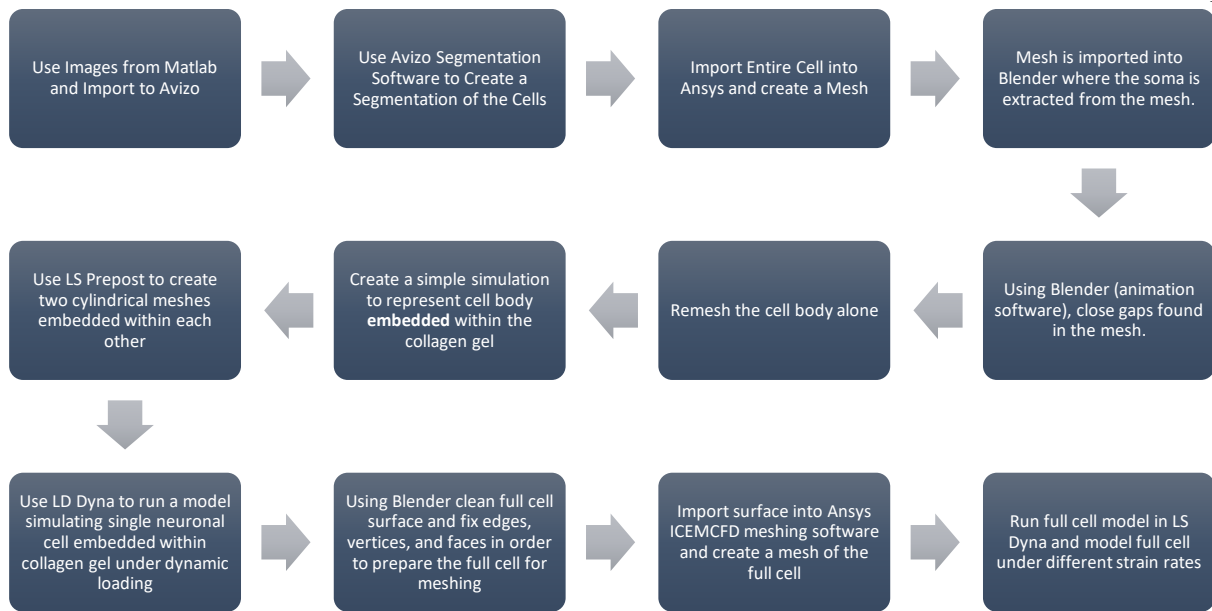


Figure 8 Single neuron highlighted using COL-I<sup>3</sup>

In order to find strain and stresses of the computational model certain steps had to be implemented and followed in order to first create the model. Table 1 and Figure 9 show the steps and flow in creating the model that made this research possible.

Table 1 Computational Modeling Process Overview

Computational Modeling Process		
Stage	Software	Purpose
Segmentation	Avizo	Create a 3D surface from extracted images of single neuron
Computer Aided Design	Blender	Design Changes
Finite Element Modeling	ANSYS ICEM-CFD	Creating and Refining Mesh
Dynamic Simulation	LS-DYNA	Develop Model



**Figure 9 Flow diagram of modeling process**

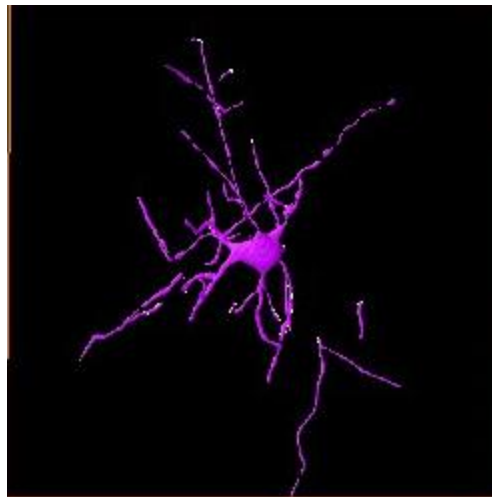
### **Creating a Segmented Surface: Avizo**

Avizo is a commercial software used for high performance 3D visualization and analysis. It is widely used in scientific and industrial data. One of the main features of Avizo that helped made this research possible was segmenting. Image segmentation refers to the partitioning of an image into many segments, or sets of pixels, known as super-pixels<sup>12</sup>. Segmentation allows users to simplify and change the representation of an image into something that is more useful<sup>12</sup>. In this research Avizo was used to create a surface from a stack of images. The Franck Lab from Brown University sent high resolution images of the controlled experiment, where a neuron was embedded in the collagen gel and experienced quasi-static loading. Using this stack of seventy-seven images and Avizo, a surface was created. Figure 10 shows some of the slices in the stack of images sent from the Franck Lab.



**Figure 10 Slices from the stack of images acquired from the Franck Lab**

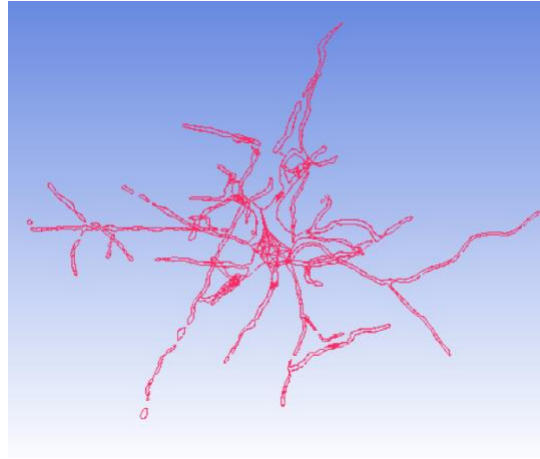
Once imported into Avizo, it is much easier to visualize the neuron. Creating the surface of a complicated structure like a neuron, including the dendrites and axon, could be very difficult. Using the Avizo “magic wand” feature and a binary (black and white) image, it only took minimal manual labor to create a surface. A picture of the original created surface can be seen in Figure 11.



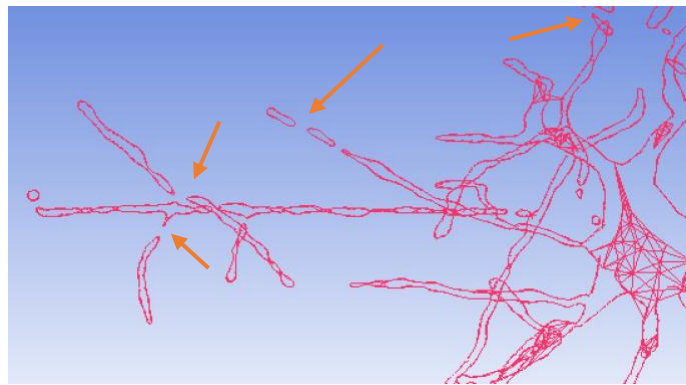
**Figure 11 Segmentation surface created using Avizo**

Since the single neuronal image was taken from a cluster of images, it made it more difficult to distinguish what parts of this surface were truly parts of the neuron and which ones were part of the neuronal network, but not involved with the single neuron. Creating a mesh from this surface would be nearly impossible. There were many gaps between dendrites and

pieces that were not associated with the neuron that were present. These would all create issues in the meshing software, ANSYS ICEM-CFD. The first import into the meshing software can be seen in Figure 12, while Figure 13 shows the gaps that would make creating a mesh impossible.



**Figure 12 Surface from Avizo imported into ANSYS ICEM-CFD meshing software**

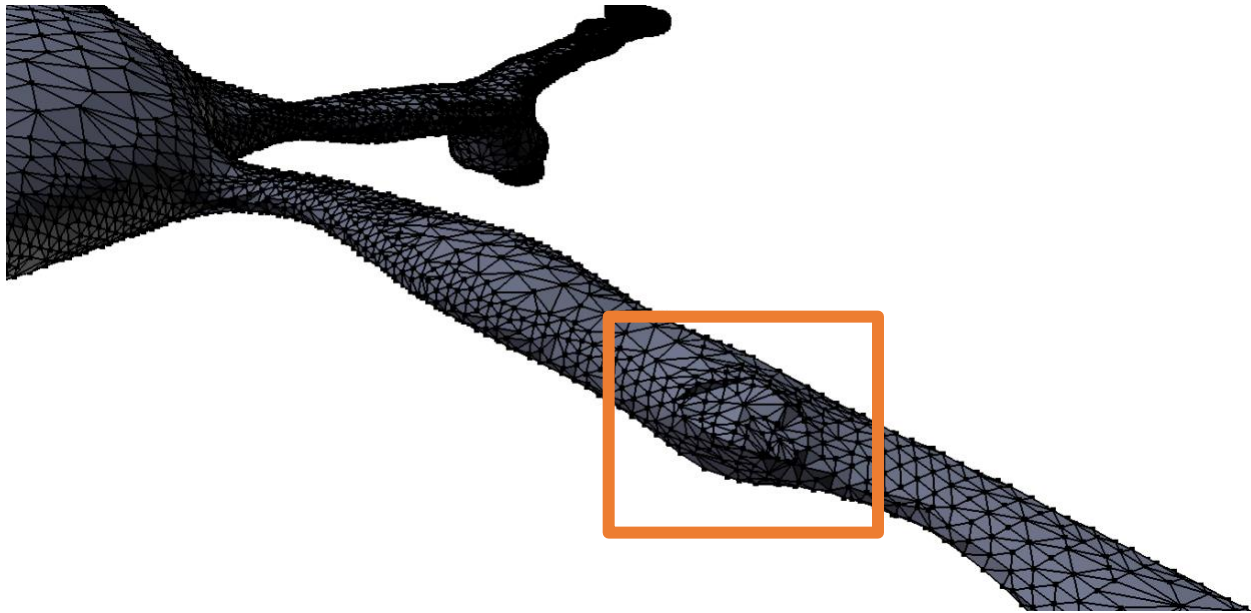


**Figure 13 Gaps in imported surface**

These gaps meant another software had to be used in order to clean up the surface. Meshes cannot be created properly in the presence of wholes, which makes meshing complex geometries one of the largest obstacles in computational modeling. This has posed a threat especially in the modeling of neurons.

## Computer Aided Design: Blender

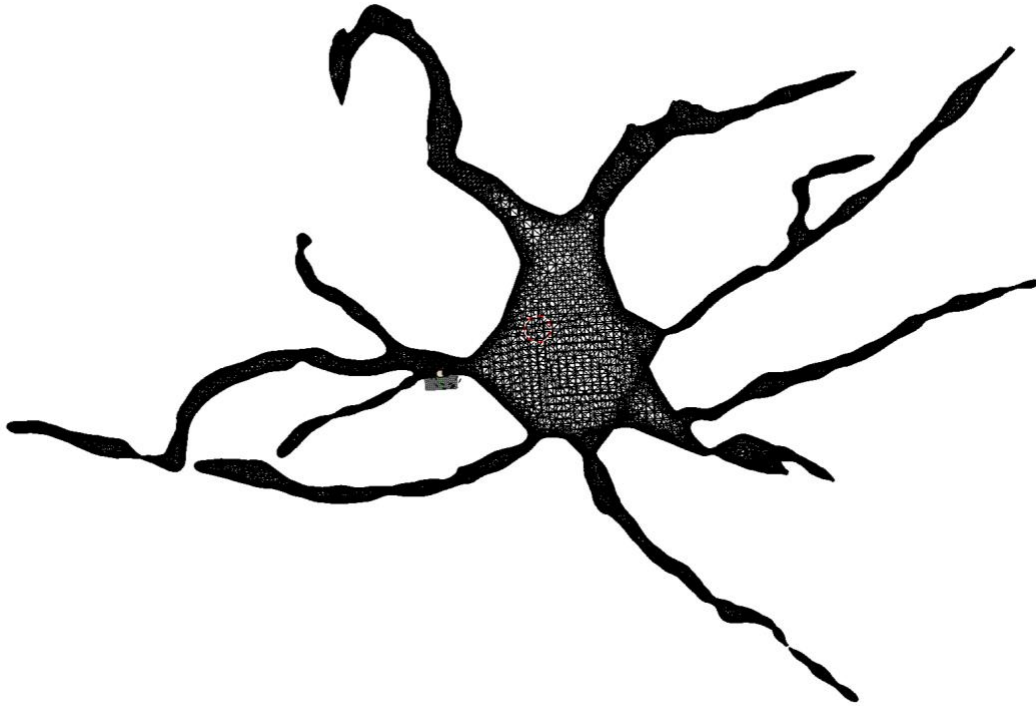
Blender is a free and open source 3D creation suite<sup>13</sup>. It is used in modeling, rigging, simulation, rendering, compositing, and motion tracking<sup>13</sup>. It is often used in video and gaming creation. For the purpose of this experiment it helped in manually editing faulty parts of the surface in order to prepare it for meshing. By going into Blender, it was much easier to see which parts of the surface were actually attached to the cell's soma. Those that were seen as unattached were thought to have been from other neurons embedded within the gel. They were deleted. Blender also has a feature where one can select all non-manifolds in a surface. Holes were fixed by connecting the surfaces that were unattached as seen in Figure 14.



**Figure 14 Fixing holes in Blender**

Through this, Blender allowed for all holes to be fixed manually. This also highlighted any edges that were uneven and sharp, which would have also created issues upon meshing. The

resultant surface can be seen in Figure 15 as seen in Blender. This created surface was exported as an STL file which is compatible with the meshing software used.

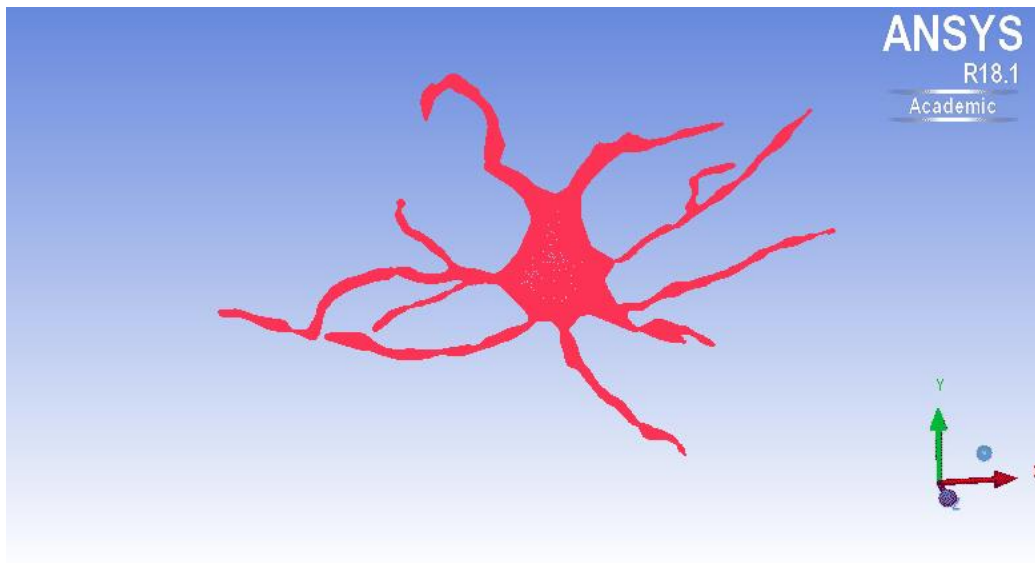


**Figure 15 Final Blender edited neuron**

### **Finite Element Meshing: ANSYS ICEM-CFD**

After fixing the issues in the surface, involved creating the finite element mesh. The meshing process began by generating an automatic hexagonal mesh. Because the mesh had been previously imported and edited in Blender several times, the mesh formed with no errors. In order to smooth the results and get the most accurate geometry we had to manipulate the size of the elements created. Computational simulation is both time consuming and very expensive so finding the ideal size that stays true to geometry but is also feasible for a timely and cost-effective experiment was crucial. It was even more important because of the scale of the

experiment. The originally experiment had thousands of neurons embedded in a 15 mm diameter gel, however looking at one neuron, whose diameter is only about 20  $\mu\text{m}$ , makes it even more important to find a balance between how course the mesh would be and if it would resemble the experimental geometry. Figure 16 shows the refined mesh where the largest element is only 1 and the smallest is 0.25. These numbers were arbitrary as they were scaled once again in pre-processing. After all meshing problems were resolved, the mesh created in ANSYS could be exported to LS-DYNA. Here is where the computational simulation would take place and material properties would be assigned.

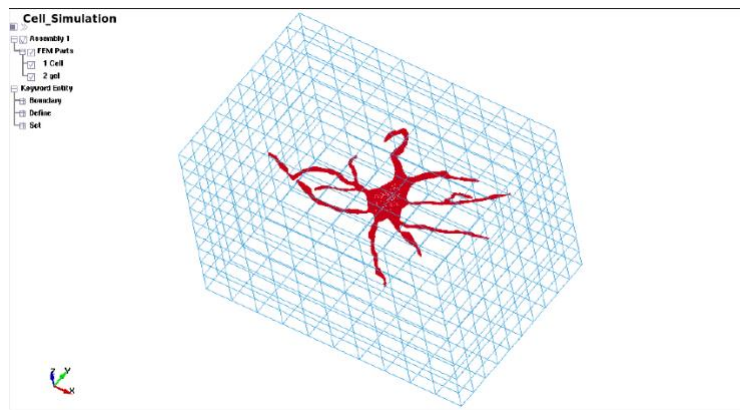


**Figure 16 Full volume rendition of mesh created in ANSYS ICEM-CFD**



## Chapter 3

### Numerical Computational Simulation: LS-DYNA



**Figure 17 Neuronal mesh embedded in a created gel**

LS-DYNA is a general-purpose finite element modeling program. It is able to replicate many complex real-world problems and is used avidly within the Computational Biomechanics Group at Penn State. LS-DYNA also has the capability of creating meshes. ANSYS usually predefines certain keywords, but in this experiment the created mesh had to be embedded within another mesh not yet created. For this research, the neuronal mesh was imported while a simple version of the collagen gel in which the experimental neurons were embedded in was created in LS-DYNA. The first step in creating the entire simulation once in LS-DYNA was actually embedding the neuron within this created gel. The geometry of the gel was simply created using the shape mesher. Once created, the entire model had to be scaled to the size of an actual neuron in order to operate correctly with the corresponding material properties. The soma, or cell body of the neuron, has a diameter of about 20  $\mu\text{m}$  which is accurate in accordance to the size of

actual cortical neurons. The gel surrounding it was then scaled down to be 100  $\mu\text{m}$  tall as seen in Figure 18.

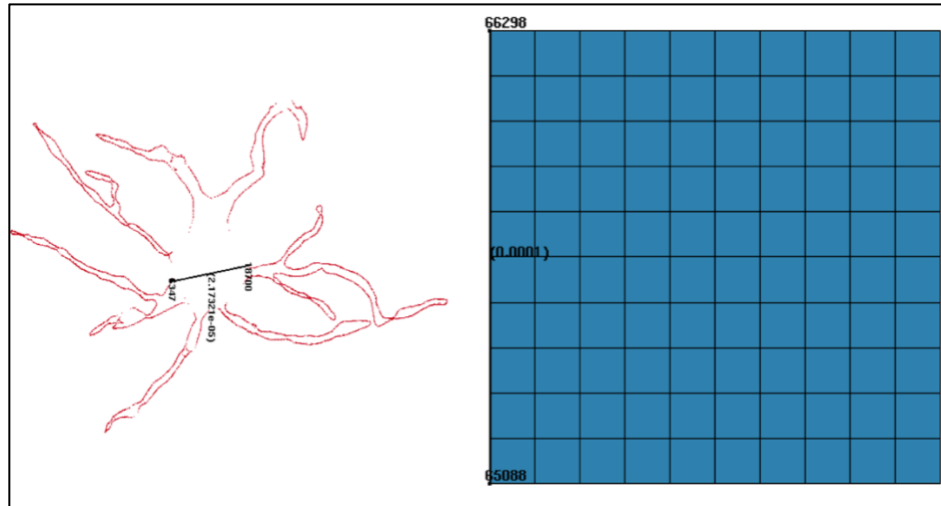


Figure 18 Dimensions of simulation

### Keyword Modification

Six important keywords were adjusted for this simulation- boundary, constrained, termination, curve, mat, and node set. The first parameter – boundary – was used in order to set the motion of the outside gel. The movement of the gel had to be set based on the conditions set forth in the original experiment and adapting this to a smaller scale simulation. The way the geometry of the neuron was imported, the gel was set to move in the negative z-direction. In the keyword function of prescribed motion set the nodes at the top of the gel were selected and free to move in this direction. Another aspect of the boundary keyword that had to be modified was the spc\_set which made the bottom of the gel constrained in only the z-direction. This way it is free to expand and deform in both the x and y directions.

The node set keyword allows one to assign different components of the simulation to be easily manipulated. When imported, the cell itself was given one node set, but in order to define

the top and bottom of the cell to different movement, these had to be created. The nodes located at the top of the gel were assigned to one node set, while those at the bottom were assigned another. This gave the model a total of three node sets. They could be easily manipulated using the separate node ID's and this helped define the curve implemented.

The entire model was based on a dynamically applied strain. The dynamically applied strain in the *in vitro* experiment was 0.3 or 30% while the peak strain rates of  $10 \text{ s}^{-1}$  and  $75 \text{ s}^{-1}$  were chosen because this matches the range of previous TBI investigations and was tested in the Franck Lab data<sup>3</sup>. The dynamic strain magnitude applied is defined by:

$$\varepsilon = \frac{l_f - l_i}{l_i} \times 100$$

Based on the initial height of  $100 \text{ }\mu\text{m}$ , the top node set of the gel was determined to move down  $30 \text{ }\mu\text{m}$  to have a final height of  $70 \text{ }\mu\text{m}$ . The strain rates are defined by:

$$\dot{\varepsilon} = \frac{v_{gel}}{d_{gel}} \text{ where } v = \frac{d_{moved}}{t}$$

This way we manipulated the time in order to achieve these strain rates and applied strains. The  $10 \text{ s}^{-1}$  simulation had a duration of 30 ms while the  $75 \text{ s}^{-1}$  simulation had a duration of 4 ms. By modifying the curve keyword, we were able to implement this into the simulation and easily move back and forth between them.

The next keyword, and probably most important, is the constrained keyword, where the LaGrange in solid was implemented into the simulation. This keyword allowed the neuronal elements and the gel elements to interact. When creating the gel after importing the neuron geometry, the two are defined as separate parts. It is this keyword that assigns the gel as the master and the neuron as the slave. This way the neuron can react to the gel's movement, therefore creating different local strains throughout the cell.

The termination keyword is crucial in determining the length of the simulation. It tells the simulation how long to run for. This can be tricky because when running simulations, it is important to note that simulation time does not correlate with real time and how long it actually takes to run a simulation.

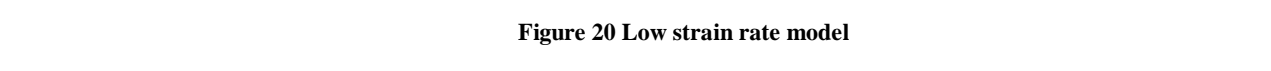
The last keyword that was modified was mat; short for material properties. Using the part IDs automatically assigned to each of the parts (the neuron and the gel), each was assigned material properties. Both of the materials possess elastic properties. The mass densities of both the gel and cell were assigned to  $1000 \text{ kg/m}^3$  because they exhibit similar properties. Young's modulus is a measure of the ability for a certain material to withstand changes in length when in tension or compression. That of the gel was 8000 Pa and 4000 Pa for the cell. The last assignment in material properties is Poisson's ratio which is the ratio of transverse strain contraction and longitudinal extension strain. The gel was assigned a Poisson's ratio of 0.485 and the cell was 0.480. These keyword adjustments can be found for the model at  $10 \text{ s}^{-1}$  and  $75 \text{ s}^{-1}$  in Appendix A.

### **Simulation Times and Completion Percentage**

A weakness this model possessed was time efficiency and completion percentage. The complex geometry and small scale of the model made it very difficult to run to completion. The highest percentage completed of the lower strain rate model was 53% and 78% for higher strain rates over 48 hours. LS-DYNA typically works more efficiently with higher strain rate models. In the future, there should be analysis as to which parts of the model could be modified in order to enhance this percentage.

## Computational Modeling Results

After the model was created the two versions were then run. As the simulation is running,



With each time-step, the neuronal geometry is not only moving with the gel, but also expanding in the y-direction. Interestingly this shows spreading. Though pathomorphology is not seen, LS-DYNA allows for both real-time visualization and graph representation. When the Franck Lab found deformities, or blebbing in the neurons subjected to dynamic loading, it was in specific regions. Figure 2 shows blebbing at major points of branching.



Figure 21 Pressure of high strain rate model

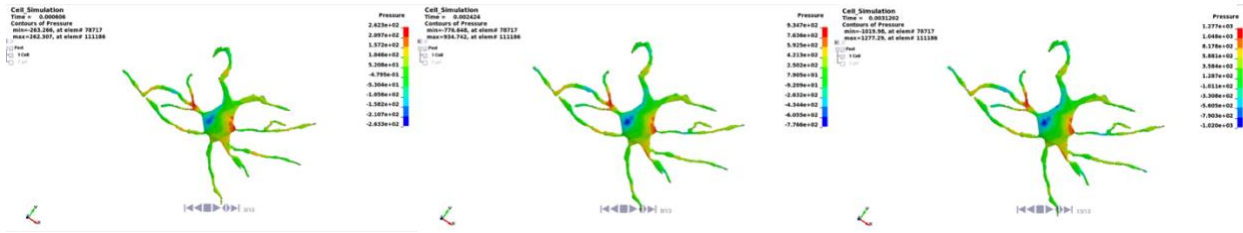


Figure 22 Pressure of low strain rate model

In both the high and low strain rate models there is an exhibition of heightened pressure in similar areas. These areas also correlate to those exhibiting blebbing. In addition, the higher strain rate exhibits higher levels of pressure which would help explain why blebbing occurs more frequently in the higher strain rate model. Certain elements continuously exhibited higher pressure, strain, and stress. Figure 23 shows a correlating graph of the pressure values for two

elements in the highlighted region. These elements were selected because throughout the time-plots, they were the two elements that exhibited the max pressure throughout.

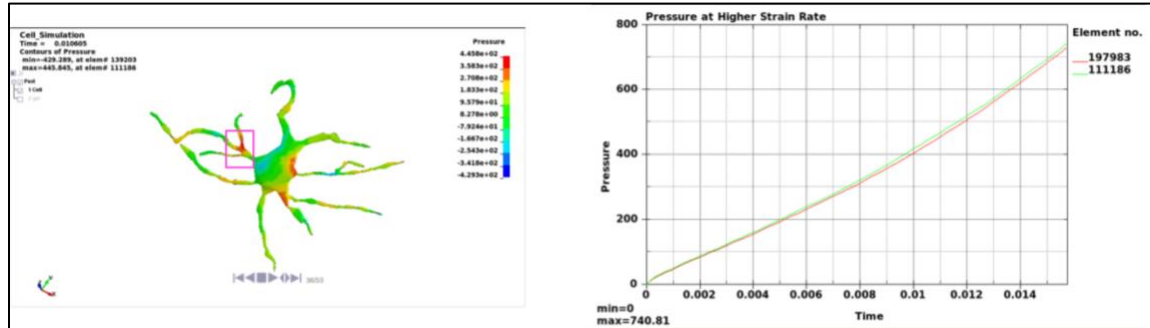


Figure 23 Pressure graph corresponding to elements in low strain rate model

The Franck Lab data primarily looked at strain and how different dynamic loading affects these areas. When comparing the same area in the high and low strain rate models there is a great increase from one to the other. This can be seen in the graphs in Figure 24. At .0001 s in the lower strain rate model the maximal principal strain is about .01, but when looking at the same time in the higher strain rate model, the resultant max principal strain is about .04, nearly four times the principal strain rate seen in the model being exposed to loading at  $10 \text{ s}^{-1}$ .

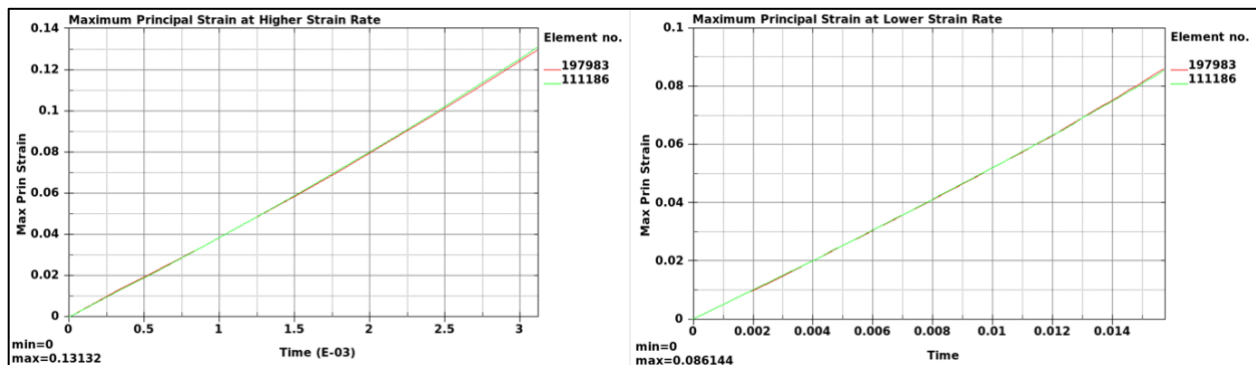


Figure 24 Comparison of high and low strain rate model principal strains

## Chapter 5

### Conclusion

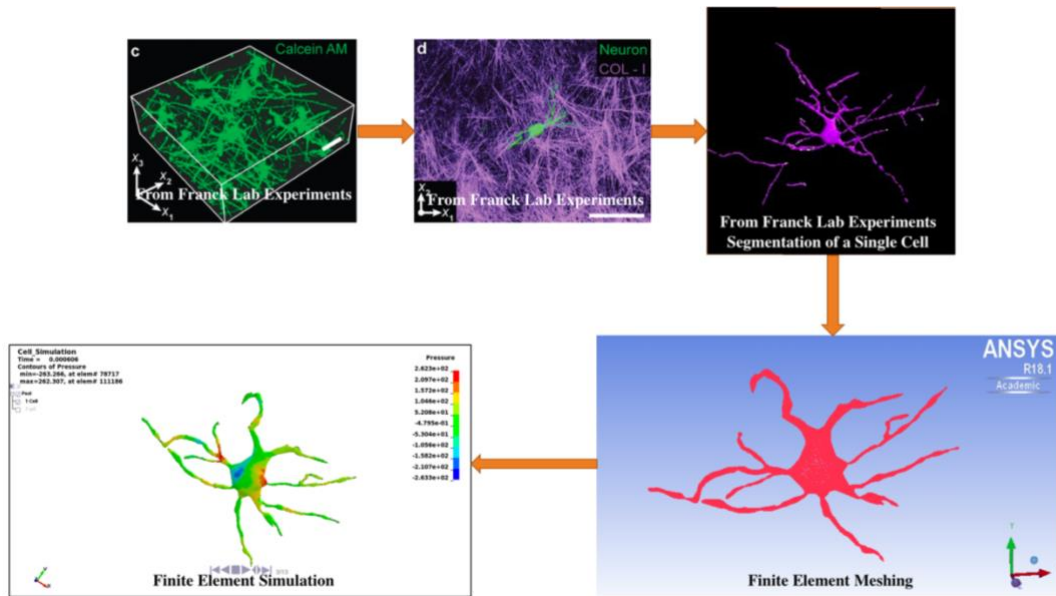


Figure 25 Visual flow diagram of modeling process

### Discussion

The computational model does not exhibit the same pathomorphology as that found in the *in vitro* experiment. This could be due to differences in material properties and the fact that the entire neuron is acting as one. A real neuron would contain different proteins and musculoskeletal components that may react to loading in a different manner. However, this model is the first step in understanding the way in which neurons react to loading. The complex geometry of these cells makes implementing these materials and other properties a challenge for the future. In addition, there was no way to determine cell death. In the *in vitro* model, fluorescence was used in order to signify whether a cell survived or not. Those cells that eventually died exhibited blebbing, especially those impacted at a higher strain rate.



Even though we were not able to visually see these outcomes, we do see similar areas of high stress, strain, and pressure where blebbing would normally occur. This validates that the model does act like the neurons in the experiment to some extent. It is a starting point in developing a more complex model. One significant finding was the extreme change in strain between the neuron impacted at a lower strain rate versus a higher strain rate. In Figure 2 it is easy to visualize how much of an impact strain rate has on the blebbing and death of neurons. Those experiencing faster loading had a nearly 4-fold increase in main principal strain. This could start to answer the question for why the experimental data found nearly a 2-fold increase in occurrence of blebbing. This can lead to a deeper understanding of the mechanical deformations and properties of single cell neurons.

### **Application**

In the future there could be an even deeper understanding of how neurons deform. Moving from a single cell to a network of cells would also resemble the experiment more adequately. Neurons act in a network and they interact constantly. Having a single cell simulation limits the understanding of how a cell would actually react in the brain. This could also help answer questions regarding TBI and the effects repetitive brain injuries have on the brain. Modeling is extremely important when it comes to the brain and cells because it is very difficult to see how a patient's cells or network of neurons have reacted to injury when the patient is still alive. Having a simulation of the impact and the possible number of impacts in the patients' history could lead to improvements in treating these injuries as well as implementing preventative care in case of future injuries.

## GitHub

GitHub is an online community that serves as an open-source version control system. It makes communicating more efficient and is easy to create a platform all in one space for multiple developers to collaborate. The GitHub for this research can be found using the following link: <https://github.com/PSUCompBio/FranckExperimentSims>. This GitHub project contains all recent files created in this research. The keyword files, mesh files, and plot results were all added to the project. In addition to this GitHub allows you to explain the project through a series of pages. These pages are very similar to the makeup of this thesis, outlining background information on Franck Lab data and all the steps taken to create the files that were uploaded to the GitHub project. Another important feature is that it allows you to document issues. In this, the issues of completion percentage and no visible deformation was explained for those who will continue the project in the future. This platform allows this research to be seen by the collaborators at Brown University, other members of the Computational Biomechanics Group, and future students who may take this project to further understand neuronal deformation.

## Appendix A

### Finite Element Analysis

#### LS-DYNA 10 s<sup>-1</sup> Simulation Keyword File

```

$# LS-DYNA Keyword file created by LS-PrePost(R) V4.3 - 14Sep2016(09:00)
$# Created on Mar-22-2018 (23:59:04)
*KEYWORD
*TITLE
$#                                     title
Cell_Simulation
$
$$$$$$$$$$$$$$$$$$$$$$$$$$$$$$$$$$$$$$$$$$$$$$$$$$$$$$$$$$$$
$      Writing Control Cards
$$$$$$$$$$$$$$$$$$$$$$$$$$$$$$$$$$$$$$$$$$$$$$$$$$$$$$$$$$$$
$
*CONTROL_CPU
$  CPUTIM
$# cputim
    0.0
*CONTROL_ENERGY
$  HEGN  RWEN  SLNTEN  RYLEN
$# hgen  rwen  slnten  rylene
    2    2    2    1
*CONTROL_HOURLASS
$  IHQ    QH
$# ihq    qh
    1    0.1
*CONTROL_OUTPUT
$  NPOPT  NEECHO  NREFUP  IACCOP  OPIFS  IPNINT  IKEDIT  IFLUSH
$# npopt  neecho  nrefup  iaccop  opifs  ipnint  ikedit  iflush
    0    3    0    0    0.0    0    0    0
$# iprtf  ierode  tet10s8  msgmax  ipcurv  gmdt  ip1dblt  eocs
    0    0    2    50    0    0.0    0    0
$# tolev  newleg  frfreq  minfo  solsig  msgflg  cdetol
    2    0    1    0    0    0    10.0

```

```

*CONTROL_TERMINATION
$ ENDTIM  ENDCYC  DTMIN  ENDENG  ENDMAS
$# endtim  endcyc  dtmin  endeng  endmas
    0.03    0    0.8    0.01.000000E8
*CONTROL_TIMESTEP
$ ENDTIM  ENDCYC  DTMIN  ENDENG  ENDMAS
$# dtinit  tssfacs  isdo  tslimt  dt2ms  lctm  erode  mslst
    10.0    0.9    0    0.0    0.0    0    0    0
$# dt2msf  dt2mslc  imslc  unused  unused  rmscl
    0.0    0    0          0.0
*DATABASE_ABSTAT
$#  dt  binary  lcur  ioopt
    0.001    0    0    1
*DATABASE_GLSTAT
$#  dt  binary  lcur  ioopt
    0.001    0    0    1
*DATABASE_MATSUM
$#  dt  binary  lcur  ioopt
    0.001    0    0    1
*DATABASE_RWFORC
$#  dt  binary  lcur  ioopt
    0.001    0    0    1
*DATABASE_BINARY_D3PLOT
$0
$#  dt  lcdt  beam  npltc  psetid
    0.0    0    0    100    0
$# ioopt
    0
*DATABASE_BINARY_D3THDT
$  dt  lcdt  beam  npltc  psetid  istats  tstart  iavg
$#  dt  lcdt  beam  npltc  psetid
    1.0    1    0    0    0
*DATABASE_BINARY_INTFOR
$  dt  lcdt  beam  npltc  psetid  istats  tstart  iavg
$#  dt  lcdt  beam  npltc  psetid
    1.0    1    0    0    0
$# ioopt
    0
*DATABASE_EXTENT_BINARY
$ neiph  neips  maxint  strflg  sigflg  epsflg  rltflg  engflg
$# neiph  neips  maxint  strflg  sigflg  epsflg  rltflg  engflg
    0    0    0    1    1    1    1    1
$# cmpflg  ieverp  beamip  dcomp  shge  stssz  n3thdt  ialemat
    0    1    0    1    1    1    2    1
$# nintsld  pkp_sen  sclp  hydro  msscl  therm  intout  nodout
    0    0    1.0    0    0    0

```

\$# dtdt resplt neipb  
0 0 0

\*BOUNDARY\_PRESCRIBED\_MOTION\_SET\_ID

\$# id heading  
1Displacement

\$# nsid dof vad lcid sf vid death birth  
1 3 2 1 1.0 01.00000E28 0.0

\*BOUNDARY\_SPC\_SET\_ID

\$# id heading  
1Sliding Bottom

\$# nsid cid dofx dofy dofz dofrx dofry dofrz  
3 0 0 0 1 1 1 1

\*SET\_NODE\_LIST\_TITLE

Bottom

\$# sid da1 da2 da3 da4 solver  
3 0.0 0.0 0.0 0.0MECH

\$#	nid1	nid2	nid3	nid4	nid5	nid6	nid7	nid8
	64978	64979	64980	64981	64982	64983	64984	64985
	64986	64987	64988	64989	64990	64991	64992	64993
	64994	64995	64996	64997	64998	64999	65000	65001
	65002	65003	65004	65005	65006	65007	65008	65009
	65010	65011	65012	65013	65014	65015	65016	65017
	65018	65019	65020	65021	65022	65023	65024	65025
	65026	65027	65028	65029	65030	65031	65032	65033
	65034	65035	65036	65037	65038	65039	65040	65041
	65042	65043	65044	65045	65046	65047	65048	65049
	65050	65051	65052	65053	65054	65055	65056	65057
	65058	65059	65060	65061	65062	65063	65064	65065
	65066	65067	65068	65069	65070	65071	65072	65073

...skipping one line

65082	65083	65084	65085	65086	65087	65088	65089
65090	65091	65092	65093	65094	65095	65096	65097
65098	0	0	0	0	0	0	0

\*PART

\$name

\$# title

Cell

\$# pid secid mid eosid hgid grav adpopt tmid  
1 1 4 0 0 0 0 0

\*SECTION\_SOLID\_TITLE

Solid

\$ id elformu aet

\$# secid elform aet  
1 1 0

\*MAT\_ELASTIC\_TITLE

```

cell
$# mid ro e pr da db not used
   4 1000.0 4000.0 0.48 0.0 0.0 0
*PART
$# title
gel
$# pid secid mid eosid hgid grav adpopt tmid

...skipping one line
   2 1 3 0 0 0 0 0
*MAT_ELASTIC_TITLE
gel
$# mid ro e pr da db not used
   3 1000.0 8000.0 0.485 0.0 0.0 0
*MAT_MOONEY-RIVLIN_RUBBER_TITLE
Gel
$# mid ro pr a b ref
   1 2200.0 0.495 560000.0 140000.0 0.0
$# sgl sw st lcide
   0.0 0.0 0.0 0
*MAT_MOONEY-RIVLIN_RUBBER_TITLE
Cell
$# mid ro pr a b ref
   2 1000.0 0.495 10000.0 2500.0 0.0
$# sgl sw st lcide
   0.0 0.0 0.0 0
*DEFINE_CURVE_TITLE
Displacement
$ id opt sfx sfy offx offy type
$# lcide sidr sfa sfo offa offo dattyp lcint
   1 0 1.0 1.0 0.0 0.0 0 0

...skipping one line
$# a1 o1
   0.0 0.0
   0.03 -2.9999999242e-05
*SET_NODE_LIST_TITLE

```

### LS-DYNA 75 s<sup>-1</sup> Simulation Keyword File

\$# LS-DYNA Keyword file created by LS-PrePost(R) V4.3 - 14Sep2016(09:00)

\$# Created on Mar-26-2018 (17:14:27)

\*KEYWORD

\*TITLE

\$# title

Cell\_Simulation

\$

\$

\$ Writing Control Cards

\$

\$

\*CONTROL\_CPU

\$ CPUTIM

\$# cputim

0.0

\*CONTROL\_ENERGY

\$ HEGN RWEN SLNTEN RYLEN

\$# hgen rwen slnten rylene

2 2 2 1

\*CONTROL\_HOURLASS

\$ IHQ QH

\$# ihq qh

...skipping one line

\*CONTROL\_OUTPUT

\$ NPOPT NEECHO NREFUP IACCOP OPIFS IPNINT IKEDIT IFLUSH

\$# npopt neecho nrefup iaccop opifs ipnint ikedit iflush

0 3 0 0 0.0 0 0 0

\$# iprtf ierode tet10s8 msgmax ipcurv gmdt ip1dblt eocs

0 0 2 50 0 0.0 0 0

\$# tolev newleg frfreq minfo solsig msgflg cdetol

2 0 1 0 0 0 10.0

\*CONTROL\_TERMINATION

\$ ENDTIM ENDCYC DTMIN ENDENG ENDMAS

\$# endtim endcyc dtmin endeng endmas

0.03 0 0.8 0.01.000000E8

\*CONTROL\_TIMESTEP

\$ ENDTIM ENDCYC DTMIN ENDENG ENDMAS

\$# dtinit tssfacs isdo tslimt dt2ms lctm erode ms1st

10.0 0.9 0 0.0 0.0 0 0 0

\$# dt2msf dt2mslc imsc1 unused unused rmscl

0.0 0 0 0.0

\*DATABASE\_ABSTAT

\$# dt binary lcur ioopt

0.001 0 0 1

\*DATABASE\_GLSTAT

...skipping one line

```
0.001    0    0    1
*DATABASE_MATSUM
$#  dt  binary  lcur  ioopt
0.001    0    0    1
*DATABASE_RWFORC
$#  dt  binary  lcur  ioopt
0.001    0    0    1
*DATABASE_BINARY_D3PLOT
$0
$#  dt  lcdt  beam  npltc  psetid
0.0    0    0    100    0
$# ioopt
0
*DATABASE_BINARY_D3THDT
$  dt  lcdt  beam  npltc  psetid  istats  tstart  iavg
$#  dt  lcdt  beam  npltc  psetid
1.0    1    0    0    0
*DATABASE_BINARY_INTFOR
$  dt  lcdt  beam  npltc  psetid  istats  tstart  iavg
$#  dt  lcdt  beam  npltc  psetid
1.0    1    0    0    0
$# ioopt
```

...skipping one line

```
*DATABASE_EXTENT_BINARY
$ neiph  neips  maxint  strflg  sigflg  epsflg  rltflg  engflg
$# neiph  neips  maxint  strflg  sigflg  epsflg  rltflg  engflg
0    0    0    1    1    1    1    1
$# cmpflg  ieverp  beamip  dcomp  shge  stssz  n3thdt  ialemat
0    1    0    1    1    1    2    1
$# nintsld  pkp_sen  sclp  hydro  msscl  therm  intout  nodout
0    0    1.0    0    0    0
$# dtdt  resplt  neipb
0    0    0
*BOUNDARY_PRESCRIBED_MOTION_SET_ID
$#  id                                     heading
1Displacement
$#  nsid  dof  vad  lcid  sf  vid  death  birth
1    3    2    1    1.0  01.00000E28  0.0
*BOUNDARY_SPC_SET_ID
$#  id                                     heading
1Sliding Bottom
$#  nsid  cid  dofz  dofz  dofz  dofrx  dofry  dofrz
3    0    0    0    1    1    1    1
*SET_NODE_LIST_TITLE
```



Bottom

...skipping one line

```
      3      0.0      0.0      0.0      0.0MECH
$#  nid1      nid2      nid3      nid4      nid5      nid6      nid7      nid8
    64978      64979      64980      64981      64982      64983      64984      64985
    64986      64987      64988      64989      64990      64991      64992      64993
    64994      64995      64996      64997      64998      64999      65000      65001
    65002      65003      65004      65005      65006      65007      65008      65009
    65010      65011      65012      65013      65014      65015      65016      65017
    65018      65019      65020      65021      65022      65023      65024      65025
    65026      65027      65028      65029      65030      65031      65032      65033
    65034      65035      65036      65037      65038      65039      65040      65041
    65042      65043      65044      65045      65046      65047      65048      65049
    65050      65051      65052      65053      65054      65055      65056      65057
    65058      65059      65060      65061      65062      65063      65064      65065
    65066      65067      65068      65069      65070      65071      65072      65073
    65074      65075      65076      65077      65078      65079      65080      65081
    65082      65083      65084      65085      65086      65087      65088      65089
    65090      65091      65092      65093      65094      65095      65096      65097
    65098          0          0          0          0          0          0          0
```

\*PART

\$name

\$# title

Cell

...skipping one line

```
      1      1      4      0      0      0      0      0
```

\*SECTION\_SOLID\_TITLE

Solid

\$ id elformu aet

\$# secid elform aet

```
      1      1      0
```

\*MAT\_ELASTIC\_TITLE

cell

```
$#  mid      ro      e      pr      da      db not used
    4  1000.0  4000.0  0.48    0.0    0.0      0
```

\*PART

\$# title

gel

```
$#  pid      secid      mid      eosid      hgid      grav      adpopt      tmid
    2          1          3          0          0          0          0          0
```

\*MAT\_ELASTIC\_TITLE

gel

```
$#  mid      ro      e      pr      da      db not used
    3  1000.0  8000.0  0.485    0.0    0.0      0
```

\*MAT\_MOONEY-RIVLIN\_RUBBER\_TITLE

Gel

\$# mid ro pr a b ref

...skipping one line

\$# sgl sw st lcld

0.0 0.0 0.0 0

\*MAT\_MOONEY-RIVLIN\_RUBBER\_TITLE

Cell

\$# mid ro pr a b ref

2 1000.0 0.495 10000.0 2500.0 0.0

\$# sgl sw st lcld

0.0 0.0 0.0 0

\*DEFINE\_CURVE\_TITLE

Displacement

\$ id opt sfx sfy offx offy type

\$# lcld sidr sfa sfo offa offo dattyp lcint

1 0 1.0 1.0 0.0 0.0 0 0

\$# a1 o1

0.0 0.0

0.004 -2.9999999242e-05

\*SET\_NODE\_LIST\_TITLE

Top

\$# sid da1 da2 da3 da4 solver

1 0.0 0.0 0.0 0.0 MECH

\$# nid1 nid2 nid3 nid4 nid5 nid6 nid7 nid8

66188 66189 66190 66191 66192 66193 66194 66195

...skipping one line

66196 66197 66198 66199 66200 66201 66202 66203

66204 66205 66206 66207 66208 66209 66210 66211

66212 66213 66214 66215 66216 66217 66218 66219

66220 66221 66222 66223 66224 66225 66226 66227

66228 66229 66230 66231 66232 66233 66234 66235

66236 66237 66238 66239 66240 66241 66242 66243

66244 66245 66246 66247 66248 66249 66250 66251

66252 66253 66254 66255 66256 66257 66258 66259

66260 66261 66262 66263 66264 66265 66266 66267

66268 66269 66270 66271 66272 66273 66274 66275

66276 66277 66278 66279 66280 66281 66282 66283

66284 66285 66286 66287 66288 66289 66290 66291

66292 66293 66294 66295 66296 66297 66298 66299

66300 66301 66302 66303 66304 66305 66306 66307

66308 0 0 0 0 0 0 0

\*SET\_NODE\_LIST\_TITLE

## BIBLIOGRAPHY

- [1] Faul, M., L. XI [1] Faul, M., L. Xi, M. M. Wald, V. Coronado, and A. M. Dellinger (2010) “Traumatic brain injury in the United States: national estimates of prevalence and incidence,” *British Medical Journal of Injury Prevention*, **16**.
- [2] Daneshvar, D. H., D. O. Riley, C. J. Nowinski, A. C. McKee, R. A. Stern, and R. C. Cantu (2012) “Long Term Consequences: Effects on Normal Development Profile after Concussion,” *Physical Medicine and Rehabilitation Clinics of North America*, **22**.
- [3] Bar-Kochba, E., Scimone, M. T., Estrada, J. B., and Franck, C. (2016) “Strain and rate-dependent neuronal injury in a 3D *in vitro* compression model of traumatic brain injury,” *Scientific Reports*, **6**.
- [4] Elmore, S. (2007) “Apoptosis: a review of programmed cell death,” *Toxicol. Pathol.* **35**, 495–516.
- [5] Ellis, E. F., McKinney, J. S., Willoughby, K. A., Liang, S. & Povlishock, J. T. A new model for rapid stretch-induced injury of cells in culture: Characterization of the model using astrocytes. *J. Neurotraum.* **12**, 325–339 (1995).
- [6] Geddes, D. M., Cargill, R. S. & LaPlaca, M. C. (2003) “Mechanical stretch to neurons results in a strain rate and magnitude-dependent increase in plasma membrane permeability,” *J. Neurotraum.* **20**, 1039–1049.
- [7] LaPlaca, M. C., Cullen, D., McLoughlin, J. J. & Cargill, R. S. (2005) “High rate shear strain of three-dimensional neural cell cultures: a new *in vitro* traumatic brain injury model,” *J. Biomech.* **38**, 1093–1105.

- [8] Cullen, D. K. & LaPlaca, M. C. (2006) "Neuronal response to high rate shear deformation depends on heterogeneity of the local strain field," *J. Neurotraum.* **23**, 1304–1319.
- [9] Kilinc, D., Gallo, G. & Barbee, K. A. (2008) "Mechanically-induced membrane poration causes axonal beading and localized cytoskeletal damage," *Exp. Neurol.* **212**, 422–430 .
- [10] "What Is CTE?" (2017) *Concussion Legacy Foundation*, The Concussion Foundation.
- [11] Barlow, Rich. (2017) "Aaron Hernandez's CTE Worst Seen in a Young Person, *Boston University*.
- [12] Pal, N. R., Pal, S. K. (1993) "A review on image segmentation techniques," *Pattern Recognition*, **26**.
- [13] "Home of the Blender Project - Free and Open 3D Creation Software." *Blender.org*, Blender, [www.blender.org/](http://www.blender.org/).

# ACADEMIC VITA

## Patricia Y. De Tomas

pattydetomas@gmail.com

---

### Education

---

#### The Pennsylvania State University

201 Old Main University Park, PA 16802

6/14-Present

Graduation Date: 5/2018

- Major: Science, Biological Sciences and Health Professions Option

---

### Experience

---

#### Researcher, Penn State Computational Biomechanics Lab, Penn State

1/15-Present

- Undergraduate research assistant supervised by Reuben Kraft, PhD
- Applied different software programs in order to body human response under extreme conditions
- Worked on projects involving modeling of ballistic impacts, craniosynostosis, and neuronal growth

#### Shadowing, Active Foot Care

6/17-Present

- Shadowed Dr. Mark Davison, DPM as he worked on many different cases involving foot care
- Dr. Danison specialized in toe care and I was able to help make observations involving gait issues

#### Shadowing, UNC Neurology Clinic, Chapel Hill, NC

6/16-8/16

- Shadowed Silvia Marovic-Plese, MD/PhD as she assessed and diagnosed Multiple Sclerosis patients
- Learned how to conduct a basic neurological exam

#### Researcher, REU in Neuroscience, UNC Chapel Hill School of Medicine

5/16-8/16

- Conducted a 10-week research project funded by the Simons Foundation Research Initiative in the lab of Mark Zylka, PhD (UNC Neuroscience Director)
- Mentored by Ralf Schmid, PhD
- Characterized neuronal brain cells of an autistic mouse model

#### Researcher, United States Army Research Laboratory, Aberdeen Proving Ground, MD

5/15-8/15

- Conducted a 10-week research project analyzing ballistic impact on porcine skull
- Supervised by Christopher Hoppel, PhD
- Operated different segmenting and meshing software such as Ansys ICEM-CFD for modeling

---

### Volunteer and Involvement

---

#### Penn State Division IA Dance Team

4/15-Present

- Practice 25+ hours/week and perform at university events and competing at the national level

#### Primary THON Chair, Penn State Dance Marathon (THON)

4/17-Present

- Serve as the primary liaison in raising money for the world's largest student run philanthropy

#### Family Relations Chair, Dance Team Lionettes, Penn State Dance Marathon (THON)

4/16-5/17

- Serve as the primary liaison between the organization and a paired family affected by pediatric cancer

#### Events Coordinator, Dancer Relations Committee, THON

10/15-Present

- Lead a group of 36 members in creating events to spread awareness of pediatric cancer
- Choreographed the Line Dance for THON volunteers in the State College Area School District

#### Millennium Scholars Peer Mentor

9/16-Present

- Mentor a group of five first year scholars about academics, research, and adjusting to college

---

### Publications & Presentations

---

Ranslow, A. N., Kraft, R. H., Shannon, R., De Tomas-Medina, "Microstructural Analysis of Porcine Skull Bone Subjected to Impact Loading." Proceedings of the 2015 ASME International Mechanical Engineering Congress and Explosion (ASME IMECE). New York: American Society of Mechanical Engineers.

#### "Characterization of Cortical Phenotypes in Ube3a T485A Autism Model Mice"

8/16

- Presented through UNC Summer Pipeline Research Program Symposium

#### "How Biomechanics are Changing the Face of Disability"

4/15

- Presented through Penn State University; Leonhard Speaking Contest Finalist

---

### Honors and Awards

---

Penn State Schreyer Honors College Scholar

8/15-Present

Penn State Millennium Scholars Program

8/14-Present

Howard Hughes Medical Institute Research Grant Recipient

5/17-8/17